J. Fluid Mech. (1997), *vol.* 330, *pp.* 61–84

Edge, cavity and aperture tones at very low Mach numbers

By M. S. HOWE

Boston University, College of Engineering, 110 Cummington Street, Boston, MA 02215, USA

(Received 13 May 1996 and in revised form 23 July 1996)

This paper discusses self-sustaining oscillations of high-Reynolds-number shear layers and jets incident on edges and corners at infinitesimal Mach number. These oscillations are frequently sources of narrow-band sound, and are usually attributed to the formation of discrete vortices whose interactions with the edge or corner produce impulsive pressures that lead to the formation of new vorticity and complete a feedback cycle of operation. Linearized analyses of these interactions are presented in which free shear layers are modelled by vortex sheets. Detailed results are given for shear flows over rectangular wall apertures and shallow cavities, and for the classical jet–edge interaction. The operating stages of self-sustained oscillations are identified with poles in the upper half of the complex frequency plane of a certain impulse response function. It is argued that the real parts of these poles determine the Strouhal numbers of the operating stages observed experimentally for the real, nonlinear system. The response function coincides with the Rayleigh conductivity of the 'window' spanned by the shear flow for wall apertures and jet–edge interactions, and to a frequency dependent drag coefficient for shallow wall cavities. When the interaction occurs in the neighbourhood of an acoustic resonator, exemplified by the flue organ pipe, the poles are augmented by a sequence of poles whose real parts are close to the resonance frequencies of the resonator, and the resonator can 'speak' at one of these frequencies (by extracting energy from the mean flow) provided the corresponding pole has positive imaginary part.

The Strouhal numbers predicted by this theory for a shallow wall cavity agree well with data extrapolated to zero Mach number from measurements in air, and predictions for the jet–edge interaction are in excellent accord with data from various sources in the literature. In the latter case, the linear theory also agrees for all operating stages with an empirical, nonlinear model that takes account of the formation of discrete vortices in the jet.

1. Introduction

The sound produced by nominally steady, high-Reynolds-number flow over an aperture or cavity in a wall often consists of a sequence of discrete tones (see Rockwell 1983 and references cited therein). The relative amplitudes of the tones depend on flow speed, and can change abruptly between distinct operating 'stages' as the speed varies. Each stage is associated with a continuous and distinct range of Strouhal number fL/U, which determines the dominant frequency f, where L is a characteristic dimension of the aperture or cavity in the flow direction and U is the free-stream speed. Transitions occur between adjacent stages of higher or lower Strouhal number, respectively, as the flow speed is increased or decreased (Rossiter 1962; East 1966; Komerath, Ahuja & Chambers 1987; Ahuja & Mendoza 1995), and the jumps usually

exhibit hysteresis, where a downward transition occurs at a lower speed than the corresponding upward jump.

Wall aperture and cavity operating stages are associated with a feedback mechanism involving the periodic formation of discrete vortices near the leading (upstream) edge (Rossiter 1962). Each vortex is convected over the opening during a time of order L/U_c, at a velocity U_c that is typically about half the free-stream speed U. An impulsive disturbance is generated when the vortex reaches the downstream edge which initiates the formation of a new vortex. The impulse takes a finite time $\approx L/c_0$ to travel back across the opening, where c_0 is the speed of sound. This naive picture accordingly implies that the frequency of vortex formation satisfies $n/f \approx L/U_c + L/c_0$, where the values $n = 1, 2, 3$, etc. correspond to the various operating stages. In practice, it is necessary to incorporate an additional frequency-dependent time delay in this equation to account for phase lags introduced by the fluid–structure interactions at the edges (Rossiter 1962; Heller & Bliss 1975). There are currently no general prediction schemes for wall aperture operating stages (and according to the vortex sheet models developed by Möhring (1975) and Durbin (1984), they do not exist), and only limited progress has been made in the direct numerical simulation at finite Reynolds numbers of unsteady shear flow over cavities (e.g. Tam & Block 1978; Bruggeman 1987; Bruggeman *et al.* 1989; Peters 1993; Hardin & Pope 1995; Kriesels *et al.* 1995).

Feedback also governs the generation of edge tones, produced (in the typical experimental arrangement) by a thin blade of air emerging from a rectangular orifice and impinging on a parallel knife-edge (Brown 1937*a*, *b*; Powell 1961; Holger, Wilson & Beavers 1977, 1980; Lepicovsky & Ahuja 1983; Blake & Powell 1986). Quasi-empirical models of the jet–edge interaction have been proposed by Curle (1953) and by Holger *et al.* (1977); the jet was assumed to evolve into a periodic vortex street whose interaction with the edge can be treated approximately by potential flow theory. By suitably adjusting the phase between vorticity production and the calculated jet motion, Holger *et al.* obtained a formula for the dependence of Strouhal number on jet thickness that is in good agreement with a broad range of experiments for all of the observed operating stages (i.e. for $n \leqslant 4$). Crighton (1992) has recently developed an asymptotic, linear theory in which the jet velocity profile is uniform and the hydrodynamic wavelength of disturbances on the jet is very much larger than the jet thickness d, yet small relative to the distance L between the edge and orifice. Crighton's analysis leads to a formula for the dependence of Strouhal number on the ratio L/d and operating stage number n that is functionally equivalent to that given by Holger *et al.*, although the numerical values of corresponding coefficients in each formula are considerably different.

Crighton's (1992) treatment of the jet–edge interaction is the first that does not depend on the introduction of empirical, adjustable parameters. His Strouhal number equation for the feedback loop is of the type first proposed by Powell (1961), and includes complex terms which can be identified with the growth of unstable waves on the jet and with the algebraic decay of impulsive pressures generated at the edge. It was asserted, however, that the complex terms must be discarded; that linear theory can only determine admissible Strouhal numbers from a phase-locking criterion expressed by the 'real form' of the frequency equation. This approach may be contrasted with that advanced by Howe (1996), who estimated from linear theory the first stage Strouhal number for wall apertures; it was argued that the complex form of the frequency equation should be retained, and that the operating Strouhal numbers observed in practice for the real, nonlinear flow correspond to the real parts of roots lying in the upper complex frequency plane. According to this hypothesis, nonlinear

mechanisms ultimately curtail the unlimited growth in time of the unstable motions, but have no significant influence on the fundamental (real) frequency. This will be the case if the convection velocity U_c is independent of amplitude, which appears to be generally true in practice (Powell 1961; Holger *et al.* 1977; Blake & Powell 1986).

In this paper the linear theory proposed by Howe (1996) is refined to determine the first four operating stages of aperture and shallow-cavity tones, and extension is made to the jet–edge interaction. In all of these cases the complex frequencies, whose real parts, we claim, correspond to the Strouhal numbers of possible operating stages, are identified with the poles of an appropriate impulse response function. For wall apertures and the jet–edge interaction, this function is the Rayleigh conductivity of the structural 'window' spanned by the shear layer or jet as influenced by the mean flow (Rayleigh 1945). An asymptotic expression is available for the conductivity of a rectangular wall aperture of large aspect ratio when the shear layer is modelled by a vortex sheet, and this is used to obtain a first approximation for the poles in the general case. The results for the jet–edge interaction are validated by comparison with an extensive body of data compiled by Holger *et al.* (1977). Furthermore, by modifying the empirical nonlinear theory of Holger *et al.* it is possible to develop a Strouhal number formula that involves one adjustable constant. When this constant is chosen to give agreement with the linear theory for any one of the operating stages, it is found that agreement is maintained for all stages.

Self-sustaining oscillations of flow over an acoustically compact wall cavity have received relatively little attention in the literature; feedback to the cavity leading edge from interactions at the trailing edge occurs instantaneously, and the motion within the cavity is effectively incompressible. For incompressible flow there can be no net volume flux through the cavity mouth, and the Rayleigh conductivity vanishes identically. In these circumstances the appropriate impulse response function is the drag coefficient for small-amplitude unsteady fluctuations in the mean flow over the cavity. Cavity resonances are determined by complex poles of the drag coefficient, and the corresponding Strouhal numbers are found to agree well with wall cavity data extrapolated to zero Mach number.

The paper is organized as follows. The general basis of the theory is outlined in §2 by detailed consideration of the rectangular wall aperture. The jet–edge problem is formulated and solved numerically in §3, and predictions compared with experimental data from several sources. An approximate treatment of the nonlinear problem is discussed (§3.3) and shown to be consistent over all operating stages with linear theory. A brief outline is given in §3.4 of the modifications necessary when the jet–edge interactions excite oscillations in a cavity resonator, such as an organ pipe. Finally, in §4 we investigate the operating stages of tones generated by flow at infinitesimal Mach number over an acoustically compact wall cavity.

2. Shear tones generated by flow over a rectangular wall aperture

2.1. *Criterion for self-sustained oscillations*

Consider high-Reynolds-number, one-sided grazing flow at infinitesimal Mach number over a rectangular aperture in a thin rigid wall. The wall coincides with the plane $x_2 = 0$ of the rectangular coordinate system (x_1, x_2, x_3) with the origin at the geometrical centre of the aperture. The mean flow is parallel to the x_1-axis in the 'upper' region $x_2 > 0$ with main stream velocity U and uniform mean density ρ_0 (see figure 1). The sides of the aperture are, respectively, of lengths L and b parallel and transverse to the mean flow, so that the aperture occupies $|x_1| < s \equiv \frac{1}{2}L, |x_3| < \frac{1}{2}b$. The shear layer over

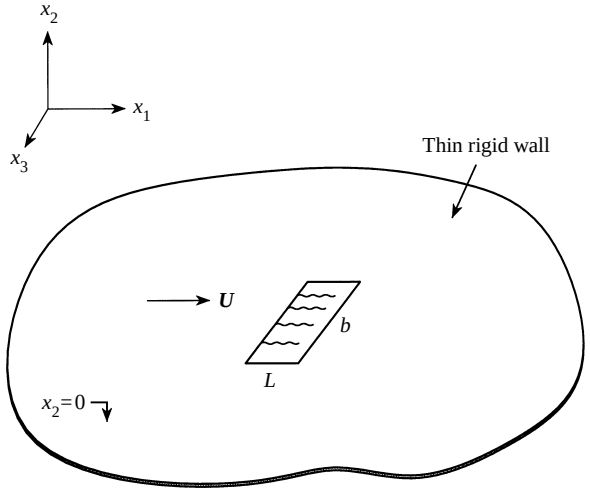

FIGURE 1. One-sided uniform flow over a rectangular aperture in a thin wall ($L = 2s$).

the aperture is assumed to be linearly disturbed by a uniform, time-dependent pressure differential $[p_0(t)] \equiv p_+(t) - p_-(t)$, where $p_\pm(t)$ are uniform pressures applied, respectively, above and below the wall. The resulting volume flux $Q(t)$ through the aperture is equal to the effective monopole source strength of sound radiated from the aperture (Pierce 1989), and is determined by the equation

$$\rho_0 \partial Q(t)/\partial t = -\int_{-\infty}^{\infty} K_R(\omega)\,[p_0(\omega)]\,\mathrm{e}^{-\mathrm{i}\omega t}\,\mathrm{d}\omega, \tag{2.1}$$

where $K_R(\omega)$ is the Rayleigh conductivity (Rayleigh 1945), which is a function of the radian frequency ω, and

$$[p_0(\omega)] \equiv (1/2\pi)\int_{-\infty}^{\infty} [p_0(t)]\,\mathrm{e}^{\mathrm{i}\omega t}\,\mathrm{d}t$$

is the Fourier component of $[p_0(t)]$ of frequency ω.

The conductivity K_R has the dimensions of length, and in the absence of mean flow, and when dissipation within the fluid and at boundaries is ignored, is determined by the shape of the aperture (it is approximately equal to $2 \times (\text{aperture area}/\pi)^{1/2}$ when the aperture aspect ratio $b/L \approx O(1)$ (Rayleigh 1945)). Viscous effects cause dissipation within the aperture, but in the presence of flow viscosity is responsible for the shedding of additional vorticity from the aperture edges, driven by the interaction of the volume flux Q with the mean flow. The conductivity $K_R(\omega)$ then becomes complex valued and strongly dependent on frequency, and the aperture motion may be unstable, its amplitude growing by extracting energy from the mean flow. These instabilities correspond to singularities of K_R occurring at complex values of ω.

It may always be assumed that the applied pressure differential $[p_0(t)]$ vanishes for $t < t_0$, say, and is non-zero only within some finite interval of time, so that $[p_0(\omega)]$ is regular in the whole of the complex frequency plane, and vanishes as $|\omega| \to \infty$. Then the causal response of the aperture flux to the applied pressure is calculated from (2.1) by requiring the path of integration to pass above any singularities of $K_R(\omega)$. For $t > t_0$ the integral is evaluated by displacing the path downwards towards the real axis, thereby capturing contributions from any singularities of $K_R(\omega)$ in $\mathrm{Im}\,\omega > 0$. According to linear theory, these contributions (if they exist) will grow exponentially with $t - t_0$,

and eventually dominate $Q(t)$. In particular, a pole in the upper frequency plane will initiate an oscillatory motion of fixed frequency whose amplitude increases exponentially. Nonlinear mechanisms will prevent unlimited growth, but will not necessarily significantly change the frequency of the oscillations, since this is determined for both the linear and nonlinear cases by the convection velocity of vortical disturbances past the downstream edge of the aperture, which experiments suggest to be hardly influenced by vortex strength (Powell 1961; Holger *et al.* 1977; Blake & Powell 1986).

We shall therefore interpret the real parts of poles of $K_R(\omega)$ in the upper half-plane as the frequencies of possible self-sustaining oscillations. In most of the cases treated in this paper $K_R(\omega)$ (and the drag coefficient of §4) is determined by numerical integration, and the existence of singularities other than poles remains an open question. It seems likely, however, that the basic physical mechanism governing the oscillations of all these systems will not differ substantially from that for the wall aperture, for which we can prove that all singularities are poles when the aspect ratio $b/L \gg 1$.

2.2. *The Rayleigh conductivity*

The equations determining the conductivity K_R of a rectangular aperture are discussed by Howe, Scott & Sipcic (1996), and it will suffice here to give only those details that are needed in §3 to study the jet–edge interaction.

For high-Reynolds-number flow, the shear layer over the aperture is replaced by a vortex sheet, and we consider time-harmonic excitation of the sheet by a uniform pressure differential $[p_0(\omega)]\,\mathrm{e}^{-\mathrm{i}\omega t}$. Let $\zeta(x_1, x_3)\,\mathrm{e}^{-\mathrm{i}\omega t}$ denote the displacement of the vortex sheet (in the x_2-direction) from its undisturbed position $x_2 = 0$. At very low Mach numbers the local motion may be regarded as incompressible; the linearized perturbation pressures above and below the plane are then given by

$$p = p_+ - \rho_0\left(\omega + \mathrm{i}U\frac{\partial}{\partial x_1}\right)^2 \int_S \frac{\zeta(y_1, y_3)}{2\pi|\boldsymbol{x}-\boldsymbol{y}|}\,\mathrm{d}y_1\,\mathrm{d}y_3 \quad (x_2 > 0), \tag{2.2a}$$

$$p = p_- + \rho_0\,\omega^2 \int_S \frac{\zeta(y_1, y_3)}{2\pi|\boldsymbol{x}-\boldsymbol{y}|}\,\mathrm{d}y_1\,\mathrm{d}y_3 \quad (x_2 < 0), \tag{2.2b}$$

where $\boldsymbol{y} = (y_1, 0, y_3)$, the integration is over the area S of the aperture, and the exponential time factor $\mathrm{e}^{-\mathrm{i}\omega t}$ is here and hereinafter suppressed. The equation of motion of the vortex sheet is obtained by equating these pressures at its undisturbed position, yielding

$$\left[\left(\omega + \mathrm{i}U\frac{\partial}{\partial x_1}\right)^2 + \omega^2\right] \int_S \frac{\zeta(y_1, y_3)}{2\pi|\boldsymbol{x}-\boldsymbol{y}|}\,\mathrm{d}y_1\,\mathrm{d}y_3 = [p_0]/\rho_0 \quad (x_2 = y_2 = 0), \tag{2.3}$$

where $\boldsymbol{x} \equiv (x_1, 0, x_3)$ is within S.

To simplify this equation, assume that vortex shedding from the leading edge ($x_1 = -s$) produces strongly correlated motion of the vortex sheet at different transverse positions x_3, and ζ may therefore be assumed to be independent of x_3. By explicitly performing the integrations with respect to y_3 and x_3, we can then write

$$\left[\sigma^2 + \left(\sigma + \mathrm{i}\frac{\partial}{\partial \xi}\right)^2\right] \int_{-1}^{1} \zeta(\eta)\,\{\ln|\xi-\eta| + \mathscr{L}(\xi, \eta)\}\,\mathrm{d}\eta = -\pi s[p_0]/\rho_0\,U^2 \quad (|\xi| < 1), \tag{2.4}$$

where

$$\sigma = \omega s/U, \quad \xi = x_1/s, \quad \eta = y_1/s,$$

and

$$\mathscr{L}(\xi,\eta) = -\ln\{b/s + [(b/s)^2 + (\xi-\eta)^2]^{1/2}\} + [1 + (s/b)^2(\xi-\eta)^2]^{1/2} - (s/b)|\xi-\eta|. \tag{2.5}$$

Inversion with respect to the second-order differential operator in ξ yields the integral equation

$$\int_{-1}^{1} \bar{\zeta}(\eta)\{\ln|\xi-\eta| + \mathscr{L}(\xi,\eta)\}\,\mathrm{d}\eta + \lambda_1 \exp(\mathrm{i}\sigma_1\xi) + \lambda_2 \exp(\mathrm{i}\sigma_2\xi) = 1 \quad (|\xi| < 1), \tag{2.6}$$

where $\sigma_1 = (\omega s/U)(1+\mathrm{i})$, $\sigma_2 = (\omega s/U)(1-\mathrm{i})$ are the Kelvin–Helmholtz wavenumbers for time harmonic disturbances of the vortex sheet, λ_1 and λ_2 are constants of integration, and $\bar{\zeta} = -(2\rho_0\omega^2 s/\pi[p_0])\,\zeta$.

This equation can be solved by collocation, as described by Scott (1995) for a vortex sheet over a circular aperture. The constants λ_1 and λ_2 are determined by imposing the Kutta condition $\zeta = \partial\zeta/\partial\xi = 0$ at the upstream edge $\xi = -1$ (Crighton 1985). Conditions at the downstream edge ($\xi = 1$) must remain unspecified, but potential theory requires that the displacement exhibit an integrable, inverse square-root singularity, which must be interpreted as the linear theory manifestation of the large-amplitude edge motion observed in experiments. The Rayleigh conductivity is then evaluated from the time-harmonic form of (2.1), by means of

$$K_R = -\tfrac{1}{2}\pi b \int_{-1}^{1} \bar{\zeta}(\eta)\,\mathrm{d}\eta. \tag{2.7}$$

The integral is a function of the dimensionless frequency σ and the aspect ratio b/L.

2.3. *Poles of $K_R(\omega)$*

When $b/L \gg 1$, it follows from (2.5) that $\mathscr{L}(\xi,\eta) \approx -\ln\{2b/s\}$. Equation (2.6) can then be solved explicitly, and (2.7) yields (Howe *et al.* 1995)

$$K_R = \frac{\pi b F_1(\omega)}{2\{F_2(\omega) + \Psi F_1(\omega)\}}, \tag{2.8}$$

where

$$\left.\begin{aligned} F_1(\omega) &= \sigma_1 W(\sigma_2)[J_0(\sigma_1) - 2W(\sigma_1)] - \sigma_2 W(\sigma_1)[J_0(\sigma_2) - 2W(\sigma_2)], \\ F_2(\omega) &= -\sigma_1 J_0(\sigma_2)[J_0(\sigma_1) - 2W(\sigma_1)] + \sigma_2 J_0(\sigma_1)[J_0(\sigma_2) - 2W(\sigma_2)], \\ \Psi &= \ln(8b/\mathrm{e}L), \quad W(x) = \mathrm{i}x[J_0(x) - \mathrm{i}J_1(x)], \end{aligned}\right\} \tag{2.9}$$

J_0 and J_1 are Bessel functions, and $\mathrm{e} \approx 2.718$ is the exponential constant.

The Bessel functions are regular everywhere, and the singularities of K_R defined by (2.8) are plainly simple poles. Now (2.1) implies that $K_R(-\omega^*) = K_R^*(\omega)$, where the asterisk denotes complex conjugate, and this permits the search for poles in $\mathrm{Im}\,\omega > 0$ to be confined to the first quadrant. An approximate formula determining these poles is obtained by considering the asymptotic forms of F_1 and F_2 as $|\sigma| \to \infty$, since it is expected that $|\sigma| > 1$ even for the first operating stage:

$$\sigma = \tfrac{1}{4}\pi(2n+1)(1+\mathrm{i}) \Big/ \left(1 - \frac{\ln\{[(4\sigma-\mathrm{i})\Psi + 2\mathrm{i}]/[1-(1-\mathrm{i})\Psi/4]\}}{2\sigma(1+\mathrm{i})}\right) \quad (n = 1, 2, 3, \ldots), \tag{2.10}$$

This indicates that the poles ultimately lie along a ray making an angle of 45° with the real axis, and that successive real and imaginary parts of $\sigma \equiv \omega s/U$ differ by about $\frac{1}{2}\pi$. A more precise determination of the poles is obtained by partitioning the first quadrant into a sequence of rectangles with sides of lengths l_R, l_I (with $l_I < \frac{1}{2}\pi$) respectively

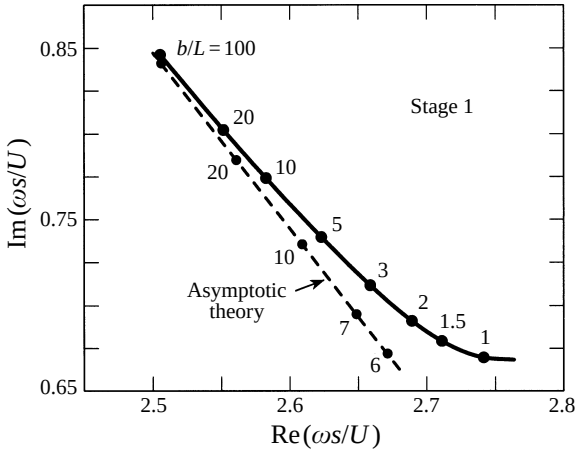

FIGURE 2. Dependence of the first stage pole on aspect ratio b/L ($L = 2s$) for a rectangular aperture in a thin wall: ——, determined by the numerical solution of equation (2.6); — — — —, determined from the asymptotic formula (2.8).

parallel to the real and imaginary axes. By trial and error l_R is taken to be sufficiently large to ensure that a pole is contained within the rectangle. This is done by defining $F(\omega) \equiv F_2(\omega) + \Psi F_1(\omega)$, and evaluating the integral $I_\gamma = (1/2\pi\mathrm{i}) \oint_\gamma \mathrm{d}F(\omega)/F(\omega)$ around the boundary γ of the rectangle; I_γ is the number of poles of $K_R(\omega)$ (zeros of $F(\omega)$) within γ (Titchmarsh 1952). The position of a pole is found to any degree of approximation by repeated subdivision of the rectangle into two equal parts followed by the evaluation of I_γ around the boundary of one of the parts. Further refinement is achieved by the Newton–Raphson method.

The broken curve in figure 2 depicts the locus of the first stage pole $\sigma \equiv \omega s/U$ of the asymptotic formula (2.8) with varying aspect ratio b/L. Only predictions for $b/L \gg 1$ are correctly given by (2.8). For arbitrary values of the aspect ratio the poles must be determined from the zeros of $1/K_R(\omega)$, where K_R is given by (2.7) from the numerical solution of the integral equation (2.6). This is efficiently accomplished by Newton–Raphson iteration, by marching from, say, $b/L = 100$, taking as a first approximation the corresponding pole of (2.8). The solid curve in figure 2 illustrates how the first stage pole calculated in this way varies with aspect ratio. The results of similar calculations performed for stages 2–4 are given in figure 3(*a*) (predictions using the asymptotic formula (2.8) are omitted). The real parts of the frequencies for the first four stages, expressed as a Strouhal number $fL/U \equiv \mathrm{Re}\,(\omega s/\pi U)$, are plotted in figure 3(*b*) as a function of b/L. For each stage the Strouhal number decreases very slowly with increasing aspect ratio, and the Strouhal numbers of successive stages differ by about $\frac{1}{2}$.

When $b/L \to \infty$, poles satisfying $|\sigma| \gg 1$ are determined by the limiting form of (2.10) as $\Psi \to \infty$, which can be written

$$8\sqrt{2}\sigma \exp\left(-\mathrm{i}(2\sigma_2 - \tfrac{1}{4}\pi)\right) = 1, \tag{2.11}$$

where $\sigma_2 = \sigma(1-\mathrm{i})$ is the (non-dimensional) wavenumber of hydrodynamic disturbances of the vortex sheet that grow exponentially with distance from the leading edge of the aperture. This equation is of the type proposed by Powell (1961) for self-sustaining oscillations controlled by feedback, and expresses the condition that the net change of phase around the loop should be a multiple of 2π and that there should be no gain in amplitude (the exponential growth of the instability wave being balanced by

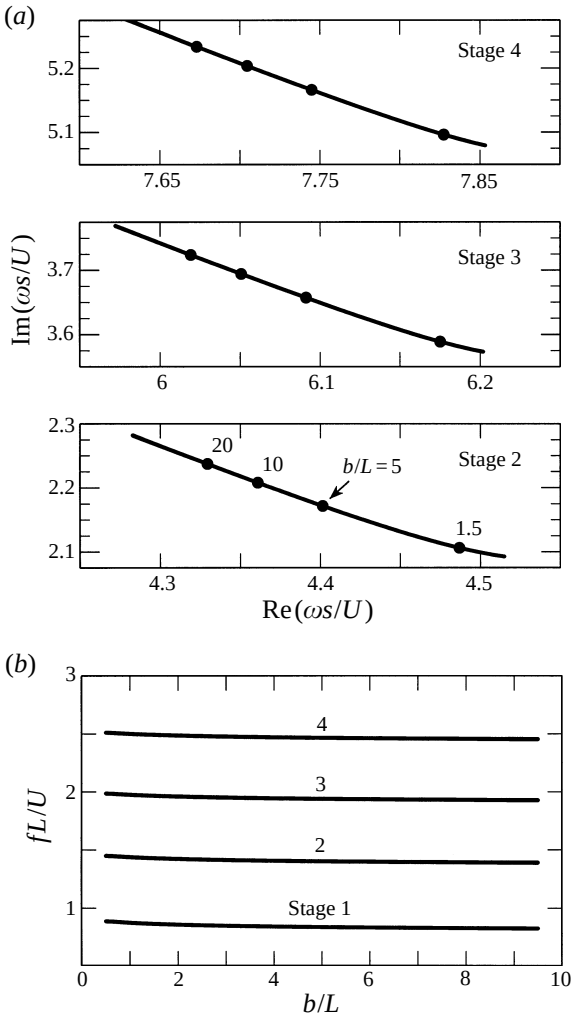

FIGURE 3. (*a*) Locus of the instability poles in stages 2–4 for a rectangular aperture in a thin rigid wall calculated from the numerical solution of equation (2.6). (*b*) Predicted dependence of the Strouhal number on aspect ratio ($L = 2s$).

an algebraic decay like $1/\sigma$ of the impulse arriving back at the leading edge from the interaction of the wave with the downstream edge). An analogous equation was given by Crighton (1992) for jet–edge interactions. However, contrary to the approach of the present paper, Crighton argued that linear theory requires σ to be real, and that it is possible to satisfy only the phase condition of (2.11), in which case

$$\sigma \equiv \omega s/U \approx \pi(n+\tfrac{1}{8})$$

in the nth operating stage. This result implies that successive Strouhal numbers fL/U differ by 1, twice the amount predicted by (2.10) (as $|\sigma| \to \infty$) and the numerical results of figure 3.

Möhring (1975) and Durbin (1984) have considered a vortex-sheet model of aperture flow for the two-dimensional case $b/L \to \infty$, subject to the condition that the motion of the sheet remains finite at the trailing edge. They concluded that there are no real resonance frequencies. Howe (1981) argued that their model is unrealistic, because it

predicts stable motion for all real frequencies and, in particular, implies that the shear flow would be incapable of exciting acoustic modes in an adjacent cavity, contrary to observation (see §3.4 below).

3. Theory of edge tones

3.1. *Linear, thin jet theory*

Let the edge tones be generated by a low-Mach-number stream of air issuing at mean velocity U from a thin-walled rectangular duct of height d and width b, where $b \gg d$ (figure 4). The duct is located symmetrically within a semi-infinite rectangular slot of equal width in the rigid plane $x_2 = 0$, with its open end a distance $L \equiv 2s$ from the transverse edge of the slot, upon which the jet impinges. The coordinate origin is taken on the centreline of the jet, midway between the orifice and the edge, with the x_1-axis in the flow direction, so that the edge is at $x_1 = s, |x_3| < \frac{1}{2}b$.

By analogy with the aperture resonances discussed in §2, the frequencies of self-sustained oscillations of the jet (in the x_2-direction) are identified with poles of the Rayleigh conductivity of the 'window' $|x_1| < s, |x_3| < \frac{1}{2}b$ connecting the 'upper' and 'lower' fluid regions. The wavelength of disturbances on the jet is assumed to be much larger than the thickness d, so that the jet displacement ζ in the x_2-direction may be assumed to be independent of x_2. The linearized equation describing sinuous motions of the jet is then

$$\rho_0 d \frac{\mathrm{D}^2\zeta}{\mathrm{D}t^2} = -[p] \quad (|x_1| < s, \quad |x_3| < \tfrac{1}{2}b), \tag{3.1}$$

where $[p]$ is the net difference in the pressures on the upper and lower surfaces ($x_2 \approx \pm\frac{1}{2}d$) of the jet, and $\mathrm{D}/\mathrm{D}t = \partial/\partial t + U\partial/\partial x_1$. The gradual increase in jet thickness d across the window is neglected.

As before, we confine attention to motions that can be regarded as incompressible in the vicinity of the jet. If $p_\pm$ are uniform, time harmonic pressures imagined to be applied to the fluid in the neighbourhood of the window in the upper and lower regions, respectively, the net perturbation pressures in $x_2 \gtrless \pm\frac{1}{2}d$ for use in (3.1) can be expressed in forms similar to equation (2.2*b*), where the integrations are over the planes $y_2 = \pm\frac{1}{2}d$, including the sections $|y_3| > \frac{1}{2}b$ of these planes to the sides of the main jet stream. When d is much smaller than either b or L, the pressures on the upper and lower surfaces of the jet may be approximated by setting $\zeta \equiv 0$ outside the window. If, in addition, the dependence of ζ on the transverse coordinate x_3 is also neglected (as in §2) these surface pressures are given by

$$p = p_\pm \mp \rho_0 \omega^2 \int_S \frac{\zeta(y_1)}{2\pi|\boldsymbol{x}-\boldsymbol{y}|}\,\mathrm{d}y_1\,\mathrm{d}y_3 \quad (|x_1| < s, \quad x_2 = y_2 = \pm\tfrac{1}{2}d, \quad |x_3| < \tfrac{1}{2}b), \tag{3.2}$$

where S is the region $|y_1| < s, |y_3| < \frac{1}{2}b$. This equation ignores possible contributions from the unsteady motions downstream of the edge ($x_1 = s$) which, for a thin, weakly perturbed jet, would be expected to be significant only near the edge. Their effect could be approximated by introducing displacement thickness waves (Crighton 1992), but such a refinement does not alter the conclusions of the present calculation, and will be ignored.

Substituting for the pressure in (3.1), and proceeding as in §2.2, the equation of motion reduces to

$$\left(\sigma + \mathrm{i}\frac{\partial}{\partial\xi}\right)^2 \zeta - \frac{2\sigma^2 s}{\pi d}\int_{-1}^{1} \zeta(\eta)\{\ln|\xi-\eta| + \mathscr{L}(\xi,\eta)\}\,\mathrm{d}\eta = \frac{s^2[p_0]}{d\rho_0 U^2}, \tag{3.3}$$

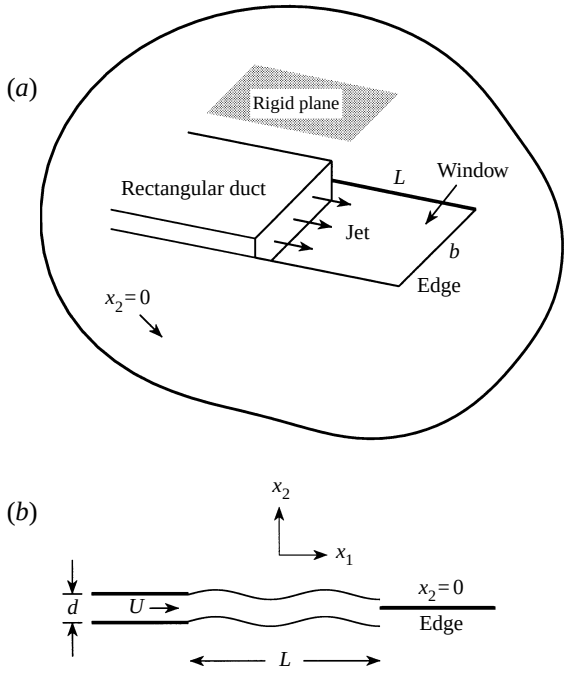

FIGURE 4. Thin, rectangular jet impinging on an edge ($L = 2s$).

where $\xi = x_1/s, \eta = y_1/s, \mathscr{L}(\xi,\eta)$ is given by (2.5), and $[p_0] = p_+ - p_-$. Crighton (1992) imposed the Kutta condition at the upper and lower edges of the jet orifice ($x_1 = -s, x_2 = \pm\frac{1}{2}d$). In the present thin jet approximation, the Kutta condition must be taken to imply the simpler condition that $\zeta = \partial\zeta/\partial\xi = 0$ as $\xi \to -1$.

Equation (3.3) can be integrated with respect to the second-order differential operator on the left-hand side by introducing the Green's function

$$G(\xi,\lambda) = -H(\xi-\lambda)\,(\xi-\lambda)\,\mathrm{e}^{\mathrm{i}\sigma(\xi-\lambda)},$$

which is a solution of $(\sigma + \mathrm{i}\partial/\partial\xi)^2 G = \delta(\xi-\lambda)$, where H is the Heaviside unit function. Then $\bar{\zeta} \equiv (\rho_0\omega^2 d/[p_0])\,\zeta$ satisfies the integral equation

$$\bar{\zeta}(\xi) + \int_{-1}^{1} K(\xi,\eta)\,\bar{\zeta}(\eta)\,\mathrm{d}\eta + \{\lambda_1 + \lambda_2\xi\}\,\mathrm{e}^{\mathrm{i}\sigma\xi} = 1 \quad (|\xi| < 1), \tag{3.4}$$

where $\sigma = \omega s/U$,

$$K(\xi,\eta) = \frac{2s\sigma^2}{\pi d}\int_{-1}^{\xi} (\xi-\lambda)\,\{\ln|\lambda-\eta| + \mathscr{L}(\lambda,\eta)\}\,\mathrm{e}^{\mathrm{i}\sigma(\xi-\lambda)}\,\mathrm{d}\lambda, \tag{3.5}$$

and λ_1 and λ_2 are integration constants chosen to ensure that $\bar{\zeta} = \partial\bar{\zeta}/\partial\xi = 0$ as $\xi \to -1$.

In terms of these definitions, the Rayleigh conductivity is given by

$$K_R(\omega)/b = \frac{s}{d}\int_{-1}^{1} \bar{\zeta}(\xi)\,\mathrm{d}\xi. \tag{3.6}$$

The result of a typical calculation for real values of the frequency ω is illustrated in figure 5, where the real and imaginary components Γ_R and Δ_R of $K_R(\omega)/b \equiv \Gamma_R(\omega) - \mathrm{i}\Delta_R(\omega)$ are plotted against $\sigma = \omega s/U$ for $L/d = 20$, $b/L = 0.5$. The general shapes of these curves are qualitatively the same as those discussed by Howe *et al.* (1996) for the conductivity of circular and rectangular apertures spanned by a vortex

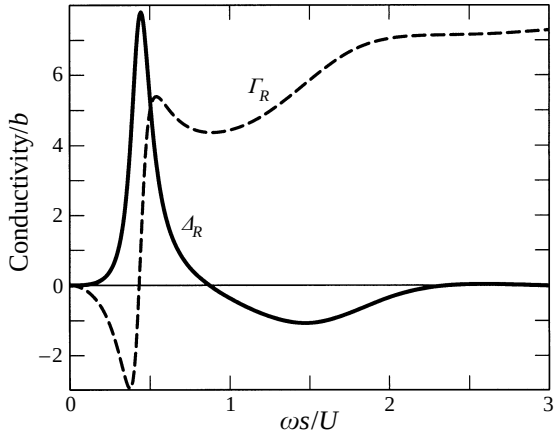

FIGURE 5. Rayleigh conductivity $K_R(\omega)/b \equiv \Gamma_R(\omega) - \mathrm{i}\Delta_R(\omega)$ for a thin jet–edge interaction when $L/d = 20$, $b/L = 0.5$ ($L = 2s$).

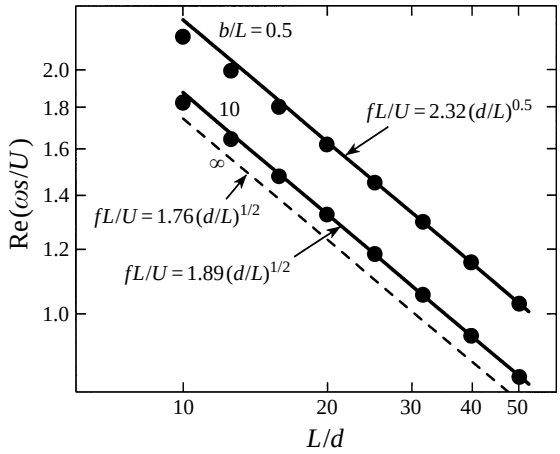

FIGURE 6. Dependence on L/d ($L = 2s$) of the real part of the stage one pole of the jet–edge interaction for different aspect ratios b/L: ●, prediction of (3.4); the straight lines are best fits of the formula (3.7) for $L/d > 20$.

sheet, where it was shown that mean flow kinetic energy is extracted by the applied pressure differential $[p_0]$ when $\Delta_R(\omega) < 0$. In figure 5 this occurs for $0.87 < \omega s/U < 2.3$.

3.2. *Calculation of edge-tone frequencies*

The Kramers–Kronig relations can be applied (in the manner described in detail by Howe *et al.* 1996) to the real and imaginary parts of K_R depicted in figure 5 for real frequencies to confirm that $K_R(\omega)$ has singularities in the upper complex-frequency plane. An extension of this method was made by Howe (1996) to obtain an approximate analytic continuation of K_R from the real axis and thereby estimate the location of the stage one pole for a wall aperture. The same procedure is applicable to jet–edge interactions, and supplies a first approximation to the first stage pole which can then be used in conjunction with the numerical solution of (3.4) and the definition (3.6) to obtain an improved approximation by Newton–Raphson iteration.

This calculation has been performed for $5 < L/d < 50$, for different fixed values of the 'window' aspect ratio b/L. Typical results are illustrated in figure 6 by the solid points in the log–log plot of $\mathrm{Re}(\omega s/U)$ against L/d for the first stage pole when

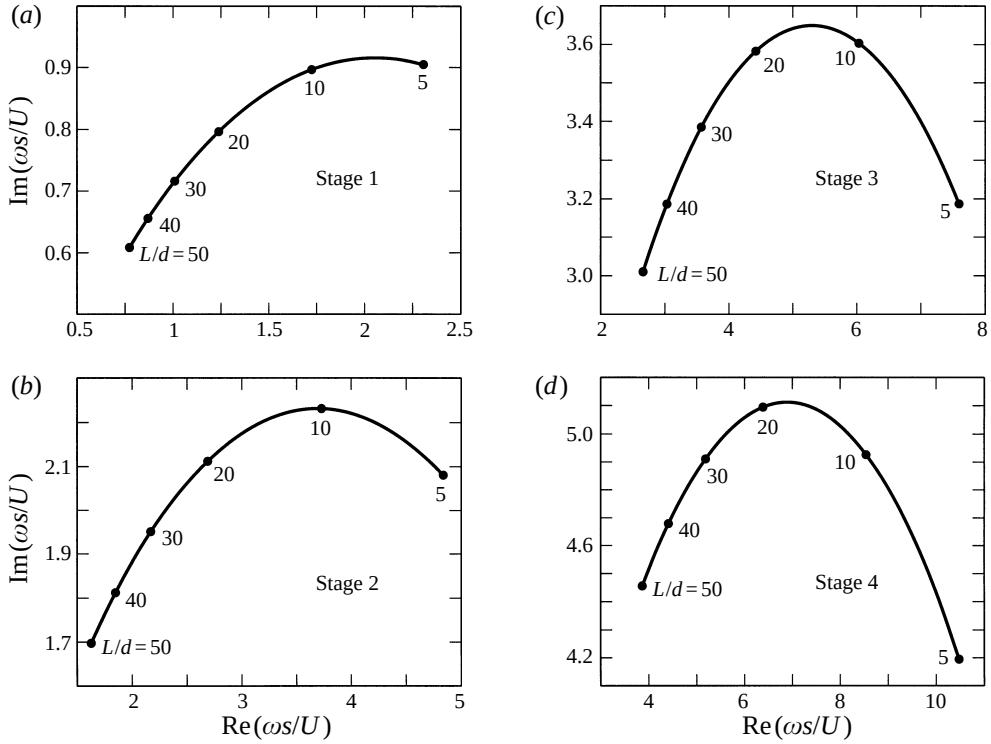

FIGURE 7. Predicted dependence on L/d ($L = 2s$) of the two-dimensional, jet–edge interaction poles for the first four operating stages.

b/L	0.5	10	500
α	2.32	1.89	1.76

TABLE 1

$b/L = 0.5$ and 10. For fixed b/L, the points are colinear when L/d is large, and the solid lines in the figure are rectilinear approximations defined by the general formula

$$fL/U = \alpha(d/L)^{1/2} \quad (L/d \gg 1), \tag{3.7}$$

where $f \equiv \mathrm{Re}\{\omega/2\pi\}$, and the coefficient α is given in table 1 for three values of b/L. Formulae similar to (3.7) were obtained by Holger *et al.* (1977) and by Crighton (1992) from considerations of two-dimensional models of the unsteady jet motion, corresponding to $b/L \to \infty$. When b/L becomes large the stage one pole tends to a limiting value whose real part varies with L/d in the manner indicated by the broken straight line in figure 6 (calculated from (3.4) by setting $b/L = 500$).

Figure 7(*a*) shows the dependence of both the real and imaginary parts of the first stage pole $\sigma = \omega s/U$ on L/d when $b/L = 500$, which we shall hereinafter refer to as the 'two-dimensional' limit. $\mathrm{Re}(\sigma)$ and $\mathrm{Im}(\sigma)$ are of the same order of magnitude, which suggests that the real and imaginary parts of the poles of successive higher-order stages will differ roughly by about $\frac{1}{2}\pi$ (as for the wall aperture). This observation facilitates the numerical determination of these poles, whose dependencies on L/d are shown in figures 7(*b*)–7(*d*) for stages two to four.

Holger *et al.* (1977) have compiled experimental data from several sources giving the

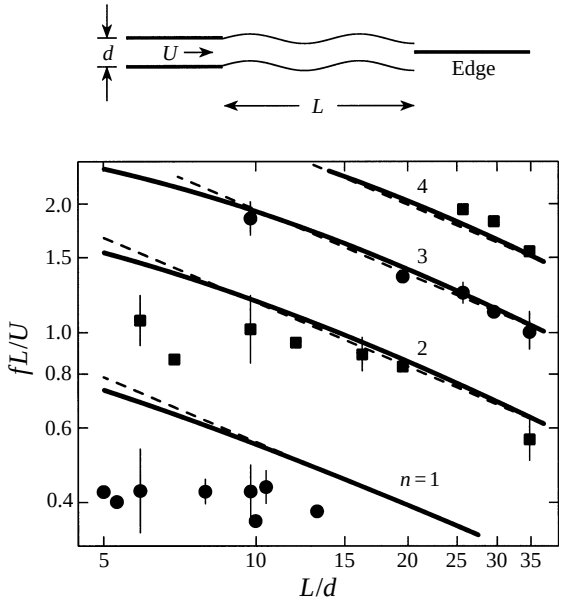

FIGURE 8. Comparison of Strouhal numbers fL/U ($\equiv \mathrm{Re}\,(\omega s/\pi U)$) from figure 7 —— for two-dimensional jet–edge interactions with representative averages of data from Holger *et al.* (1977). The broken lines are predictions of (3.18).

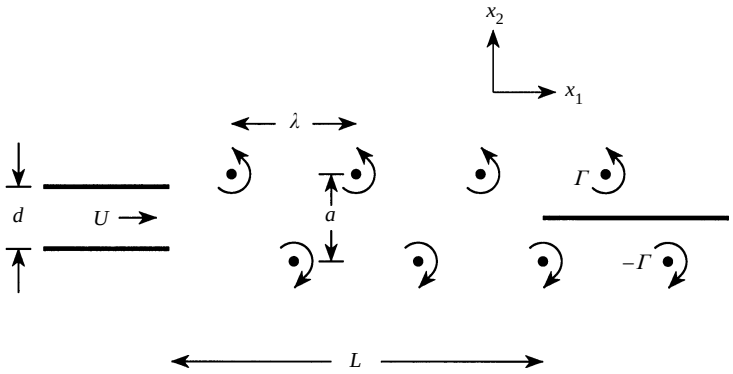

FIGURE 9. Discrete vortex model of the jet–edge interaction.

dependence of Strouhal number on L/d for the first four operating stages (the only ones observed in practice). Representative averages of this data are plotted as solid circles and squares in figure 8; any significant spread about the average is indicated by a vertical bar through a data point. The solid curves are predictions of $fL/U \equiv \mathrm{Re}\,(\omega s/U\pi)$ from figure 7 (for the 'two-dimensional' interaction), which are in excellent agreement with experiment except perhaps for stage 1, where the data are confined to the region $L/d < 10$, and where the validity of thin jet theory is questionable.

3.3. *Compatibility of linear and nonlinear theories*

Additional support for the predictions of §3.2 is obtained from a comparison with a nonlinear theory proposed by Holger *et al.* (1977). The jet is assumed to evolve into a fully developed street of vortices of alternating sign convecting towards the edge at constant speed U_c (figure 9), which is in rough accord with experiment provided the

Reynolds number Ud/ν (ν being the kinematic viscosity) is smaller than about 2000–3000. In a locally two-dimensional approximation, the vortex street is represented by line vortices of circulations $\pm\Gamma$ ($\Gamma > 0$), with vorticity distribution

$$\boldsymbol{\Omega}(\boldsymbol{x},t) \approx \sum_{n=-\infty}^{\infty} \Gamma(\delta(x_2-\tfrac{1}{2}a)\,\delta[x_1+s-U_c(t-n/f)] - \delta(x_2+\tfrac{1}{2}a)\,\delta[x_1+s-U_c\{t-(n+\tfrac{1}{2})/f\}])\,\boldsymbol{k} \quad (x_1 > -s, \quad |x_3| < \tfrac{1}{2}b), \tag{3.8}$$

where a is the vertical distance between the two rows of vortices, $\lambda \equiv U_c/f$ is the distance between neighbouring vortices in the same row, f is the fundamental frequency of the motion, and $\boldsymbol{k}$ is a unit vector in the x_3-direction (out of the plane of the paper in figure 9). According to (3.8) the nth vortex in the upper row appears spontaneously in the neighbourhood of the jet orifice at time $t = n/f$ and proceeds to drift towards the edge at constant speed U_c, although in practice the vortices actually form between one and three hydrodynamics wavelengths downstream.

Careful measurements in water (Brown 1937*a*, *b*; Holger *et al.* 1977) indicate that

$$a/\lambda \approx 0.5, \quad U_c/U \approx 0.945(fd/U)^{1/3}. \tag{3.9a, b}$$

The second of these relations is also obtained by equating the momentum flux of the jet at the orifice to that of the vortex street (Holger *et al.* 1977); the usual formula for the translational velocity of the street (Lamb 1932) then yields

$$\Gamma/Ud \approx 1.95/(fd/U)^{1/3}. \tag{3.10}$$

To use this model to calculate the Strouhal number fL/U of each operating stage, the interaction of the vortex street with the edge must be related to the formation of the vortices. Let v_2 denote the x_2-component of the perturbation velocity produced on the jet axis near the orifice by this interaction. Suppose there exists a phase lag $2\pi\theta$ between the formation of a vortex in the upper row of the street and the beginning of the half-cycle during which v_2 is positive. Then for the fundamental mode of frequency f we can then write

$$v_2 = v_0 \sin[2\pi(ft-\theta)], \tag{3.11}$$

where $v_0 > 0$ does not depend on time. This velocity must be determined by the interaction with the edge of the corresponding Fourier component of the vorticity (3.8), which can be written

$$\boldsymbol{\Omega}(z,f) = \frac{2\Gamma f}{U_c}(\delta(x_2-\tfrac{1}{2}a)+\delta(x_2+\tfrac{1}{2}a))\cos[2\pi f\{t-(x_1+s)/U_c\}]\,\boldsymbol{k}, \quad z = x_1+\mathrm{i}x_2. \tag{3.12}$$

The velocity potential (z,f) associated with the vorticity $\boldsymbol{\Omega}(z,f)$ can be evaluated by the conformal transformation $Z = Z(z)$ of the z-plane, cut along rays corresponding to the upper and lower walls of the jet duct and the edge, onto $\mathrm{Im}\,(Z) > 0$, and formally expressed as the integral

$$(z,f) = \mathrm{Re}\left(\frac{-\mathrm{i}}{2\pi}\int \Omega(z',f)\,[\ln\{Z(z)-Z(z')\}-\ln\{Z(z)-Z^*(z')\}]\,\mathrm{d}y_1\,\mathrm{d}y_2\right), \quad z' = y_1+\mathrm{i}y_2. \tag{3.13}$$

Now the experimental data shown in figure 8 suggests that $2\pi fL/U_c \gg 1$ for all operating stages. The value of this integral is therefore dominated by contributions from the vicinities of $z' = \pm s$, where $Z(z')$ is respectively singular and close to

singularities, and can be estimated by expanding the term in the square brackets of the integrand about these points (see, e.g. Lighthill 1958). However, the vorticity (3.12) is a proper representation of the flow only near $z' = s$; discrete vortices are not present near the orifice, where the motion must actually by smooth in accordance with the Kutta condition. The irrotational velocity v_2 near the orifice produced by the interaction of the jet with the edge is therefore correctly estimated by including only those contributions to the integral from the vicinity of $z' = s$, which is easily done when $2\pi fL/U_c \gg 1$. Furthermore, near $z = s$, and when $L \gg d$, the transformation $Z(z)$ may be approximated by

$$Z = z/s + (z^2/s^2 - 1)^{1/2}, \tag{3.14}$$

which maps the z-plane cut along the real axis from $\pm s$ to $\pm\infty$ onto $\mathrm{Im}\,(Z) > 0$.

It may be verified by direct calculation that in order to calculate the phase of v_2 near the jet orifice, it is sufficient to take $a = 0$ in the delta-functions of (3.12), since a non-zero value of a affects only the amplitude. Thus, in (3.13) we expand $Z(z')$ given by (3.14) about $z' = s$, and for z near the orifice and $d \ll L, Z(z)$ (given by the same formula) is expanded about the jet orifice at $z = -s$, to obtain

$$v_2 \approx \frac{\Gamma}{4\pi^2 (fs/U_c)^{1/2} (s^2 - x_1^2)^{1/2}} \sin\left[2\pi f(t - L/U_c) + \tfrac{1}{4}\pi\right]. \tag{3.15}$$

Comparing this with (3.11), it follows that

$$fL/U_c = n + \tfrac{1}{8} + \theta,$$

for integer values of n, and equation (3.9*b*) then implies that the Strouhal number stages are given by

$$fL/U \approx 0.92(d/L)^{1/2} (n + \tfrac{1}{8} + \theta)^{3/2} \quad (n = 1, 2, 3, \ldots). \tag{3.16}$$

A formula of this type which agrees well with the data of figure 8 was given by Holger *et al.* (1977) where, however, the phase θ was required to be a function θ_n of the stage number n, namely, $\theta_1 = 0.275$, $\theta_2 = 0.225$, $\theta_3 = 0.375$. Crighton's (1992) linear theory yields the following equation for the Strouhal number (analogous to equation (2.11) for the wall aperture):

$$4\pi(SL/d) \exp\left(-2\mathrm{i}[(L/d)\, S^{2/3} \mathrm{e}^{-\mathrm{i}\pi/3} - \tfrac{5}{8}\pi]\right) = 1, \tag{3.17}$$

where $S = \omega d/2U$. According to Crighton, S must be regarded as real and determined by equating the phase of the left-hand side to an integral multiple of 2π. This also yields equation (3.16), but with the factor 0.92 replaced by 5.01 and with $\theta = -\frac{1}{2}$. Thus, Crighton's formula has the correct formal structure, in particular it predicts the correct dependence of Strouhal number on d/L, but it greatly overestimates the interstage jumps, and the Strouhal numbers for $n = 1$ are about 60 % too large.

If the alternative hypothesis of the present paper is applied to (3.17) it is more usefully expressed as the following equation for the complex frequency $\sigma \equiv \omega s/U$ of successive operating stages,

$$\sigma = \frac{\pi\mathrm{i}(d/L)^{1/2} \{\pi(n - 3/8)\}^{3/2}}{[1 - \exp(5\pi\mathrm{i}/6) \ln(4\pi\sigma)/\{2(L/d)\, \sigma^2\}^{1/3}]^{3/2}} \quad (n = 1, 2, 3, \ldots).$$

However, the solutions of this equation yield totally unacceptable Strouhal numbers $fL/U \equiv \mathrm{Re}\,(\sigma/\pi) < 0$.

The argument of §2.1 implies that Strouhal numbers predicted by linear and nonlinear theories should be the same, and therefore that (3.16) should be consistent

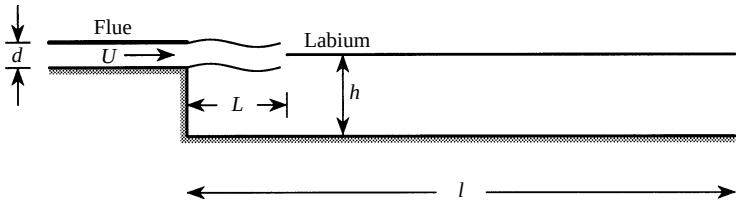

FIGURE 10. Schematic flue organ pipe.

with the theory of §3.2. According to figure 6, the first stage Strouhal number is given approximately by $fL/U = \alpha(d/L)^{1/2}$ when L/d is large, where α is constant, and the solid curves in figure 8 indicate that the same conclusion is approximately true for the higher-order predictions. The asserted equivalence of linear and nonlinear theories therefore requires that $\alpha \equiv 0.92(n+\frac{1}{8}+\theta)^{3/2}$ for a unique value of the phase shift θ. When θ is chosen to make linear and nonlinear theories agree for $n = 1$ (by taking $\alpha = 1.76$, from table 1) we find $\theta \approx 0.42$, and (3.16) becomes

$$fL/U \approx 0.92(d/L)^{1/2}(n+0.54)^{3/2}. \tag{3.18}$$

Predictions of this formula (the dashed lines in figure 8) agree precisely with linear theory in the thin jet limit $L/d \gg 1$. The conclusion that $\theta \approx 0.42$ implies that a vortex in the upper shear layer of the jet may be regarded as released from the orifice shortly before the cross-velocity v_2 goes negative.

3.4. *Edge tones coupled to a resonator*

The complex poles of the Rayleigh conductivity generally do not determine the tones generated when the jet–edge interaction occurs in the neighbourhood of the mouth of a large cavity resonator. This can be seen by consideration of the idealized model of a flue organ pipe depicted in figure 10, consisting of a uniform pipe of length l and rectangular cross-section $h \times b$ (the transverse dimension b being into the paper in the figure) open at both ends. Acoustic resonances of the pipe are excited by a nominally steady, thin jet of air from the flue impinging on the sharp edged *labium*. The distance L between the flue exit and the edge is very much smaller than the pipe length l, and is usually smaller than the cross-sectional dimensions h and b. In the thin jet approximation (3.1), an integral equation of motion of the jet is easily derived in a form similar to (3.4) with account taken of the local geometry of the mouth. The numerical predictions from this equation of the conductivity of the mouth in the presence of the jet are qualitatively the same as for the jet–edge 'window' of figure 4, and it will therefore suffice to refer, where necessary, to explicit results given previously for this simpler case.

The resonance frequencies of the organ pipe are found by equating to zero the *acoustic impedance* of the mouth (Pierce 1989). This may be broken down into two components, one representing the impedance of the mouth as influenced by the jet (whose reciprocal is the Rayleigh conductivity) and the second being the effective impedance of the pipe at a point just within the mouth in the absence of the jet. The reciprocal of the latter may be termed the Rayleigh conductivity K_c, say, of the pipe cavity entrance, and includes the influence of acoustic modes within the pipe and the radiation of sound into the ambient fluid. For the pipe of figure 10, open at both ends, it is given approximately by

$$K_c = 1/(\mathrm{i}\kappa_0/4\pi + \tan\{k(l+l'+\mathrm{i}\kappa_0 A/4\pi)\}/kA),$$

where $\kappa_0 = \omega/c_0$ is the acoustic wavenumber (c_0 being the speed of sound), $A = hb$ is the cross-sectional area of the pipe, and l' is the 'end correction' at the remote open end (at $x_1 = l$, say). The wavenumber $k = \kappa_0 + \mathrm{i}\alpha_0$, where $\alpha_0 > 0$ is a correction that accounts for boundary-layer losses at interior walls of the pipe.

If K_R denotes the conductivity of the mouth in the presence of the jet (defined for incompressible flow as in §2.1), the net impedance of the mouth is $1/K_R + 1/K_c$. In general, this has complex zeros in $\mathrm{Im}\,(\omega) > 0$ near the poles of $K_R(\omega)$ that determine the Strouhal numbers of the free jet–edge interaction. In addition, however, there exist zeros close to the poles of K_c; they are near the real axis, and correspond to acoustic modes in the pipe as modified by the jet. For the lower-order pipe modes they satisfy

$$\sin\left(k[l + l' + A\{1/K_R + \mathrm{i}\kappa_0/2\pi\}]\right) = 0.$$

The magnitude of K_R is comparable to b, and this equation is valid provided $A/K_R l \sim h/l \ll 1$, which is usually the case in organ pipes and recorder-like instruments. The solutions are given approximately by

$$\omega(l + l')/c_0 \approx n\pi(1 - \mathrm{i}(\alpha_0/\kappa_0) - [A/(l + l')][1/K_R + \mathrm{i}\kappa_0/2\pi]) \quad (n = 1, 2, 3, \ldots),$$

where the right-hand side is evaluated at $\omega(l + l')/c_0 = n\pi$. Acoustic oscillations will be self-sustained (extracting energy from the jet), and the pipe will 'speak', provided

$$\mathrm{Im}\,(1/K_R) < -\kappa_0/2\pi - [(l + l')/A]\,(\alpha_0/\kappa_0) \quad \text{at} \quad \omega(l + l')/c_0 = n\pi. \tag{3.19}$$

This is the linear theory condition that power supplied to the oscillations by the jet exceeds that dissipated by radiation from the ends of the pipe and by interior boundary-layer losses. Referring to figure 5, self-excitation can only occur when $\sigma \equiv \omega s/U$ lies within the interval where the imaginary component of the conductivity $\Delta_R < 0$. Since $\omega \approx n\pi c_0/(l + l')$, the pipe can speak at this frequency provided the inequality (3.19) can be satisfied in a subinterval of the range of σ wherein $\Delta_R < 0$, and (3.19) therefore determines the jet velocity interval (if any) within which oscillations are possible (see Howe (1981) for an example of this type of calculation).

4. The shallow wall cavity

Turn attention now to the estimation of the resonance frequencies of a shallow, acoustically compact, rectangular wall cavity ('cut-out') of the type illustrated in profile in figure 11(*a*). This subject has an extensive literature for cases of finite mean flow Mach numbers $M \equiv U/c_0$ (typically greater than about 0.2) because of its relevance to vibration problems experienced by exposed aircraft structures (Rossiter 1962; Tam & Block 1978; Ahuja & Mendoza 1995). Theoretical progress has been limited, however, and none of the existing models is applicable at infinitesimal Mach number, when the depth l is very much smaller than the acoustic wavelength (Burroughs & Stinebring 1994).

Let the cavity have dimension L ($\equiv 2s$) in the mean stream direction and b in the transverse direction (out of the plane of the paper in figure 11*a*), and take the coordinate origin in the centre of the cavity mouth. At very small Mach numbers the acoustic pressure at large distances from the cavity is given by

$$p(\boldsymbol{x}, t) \approx \frac{\rho_0}{2\pi|\boldsymbol{x}|}\frac{\partial}{\partial t}\int_{-\infty}^{\infty} v_2(\boldsymbol{y}, t - |\boldsymbol{x} - \boldsymbol{y}|/c_0)\,\mathrm{d}y_1\,\mathrm{d}y_3 \quad \text{as} \quad |\boldsymbol{x}| \to \infty. \tag{4.1}$$

As the frequency of the sound becomes very small (smaller than the Helmholtz resonance frequency (Pierce 1989)), the motion within the cavity may be regarded as

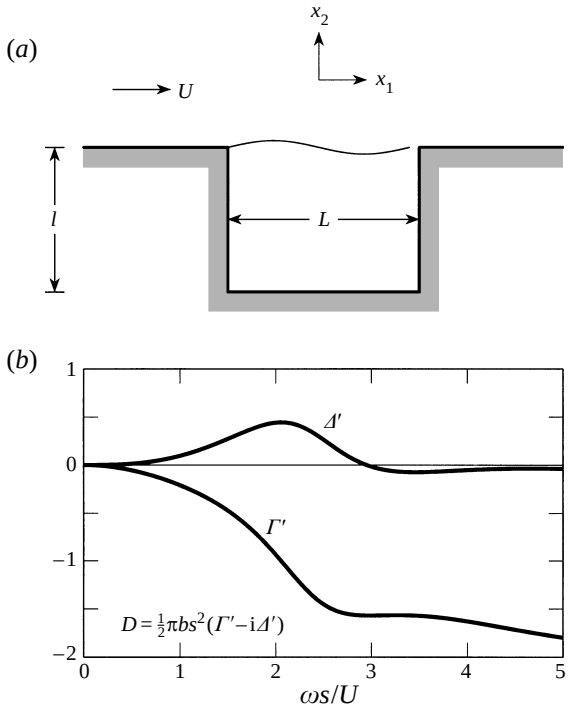

FIGURE 11. (*a*) Rectangular wall cavity. (*b*) Real and imaginary parts of the drag coefficient $D(\omega)$ defined by (4.3) for real ω when the cavity aspect ratio $b/L = 1$ ($L = 2s$).

incompressible, and the net volume flux Q through the mouth vanishes. The cavity must therefore radiate as a dipole, rather than a monopole, whose pressure field is determined by the first non-zero term in the expansion of the integrand of (4.1) in powers of $\boldsymbol{y}/c_0$:

$$p(\boldsymbol{x}, t) \approx \frac{x_j}{2\pi c_0 |\boldsymbol{x}|^2} \frac{\partial F_j}{\partial t}(t - |\boldsymbol{x}|/c_0) \quad (|\boldsymbol{x}| \to \infty),$$

where

$$F_j = \rho_0 \int_{-\infty}^{\infty} y_j \frac{\partial v_2}{\partial t}(\boldsymbol{y}, t)\, \mathrm{d}y_1\, \mathrm{d}y_3 \quad (j = 1 \text{ or } 3). \tag{4.2}$$

$\boldsymbol{F}$ is just the unsteady force exerted on the fluid, and F_1 is the drag.

In steady flow (when $Q \equiv 0$) a cavity drag cannot be induced by a uniform, time-dependent pressure $p_0(t)$ applied (in $x_2 > 0$) above the cavity. Instead, it is necessary to excite the cavity shear layer by a uniform, tangential pressure force $-\partial p_0/\partial x_j$. If this is applied in the mean flow direction (the x_1-direction), then $\boldsymbol{F} \equiv (F_1, 0, 0)$, and by analogy with (2.1) we can write, for linearly disturbed motion of the shear layer,

$$F_1(t) = -\int_{-\infty}^{\infty} D(\omega)\, \partial p_0(\omega)/\partial x_1\, \mathrm{e}^{-\mathrm{i}\omega t}\, \mathrm{d}\omega, \tag{4.3}$$

where $D(\omega)$ is a suitable drag coefficient. The frequencies of possible self-sustained radiation from the cavity correspond to poles of $D(\omega)$ in $\mathrm{Im}\,(\omega) > 0$.

Approximate the high-Reynolds-number shear layer over the mouth by a vortex

sheet, whose displacement ζ from $x_2 = 0$ is independent of the transverse coordinate x_3. Then (4.2) and the definition (4.3) imply that

$$D(\omega) = \frac{\rho_0 \omega^2 b}{p_0'(\omega)} \int_{-s}^{s} y_1 \zeta(y_1)\, \mathrm{d}y_1, \tag{4.4}$$

where $\zeta(y_1)$ here denotes the displacement produced by the uniform time harmonic pressure gradient $p_0'(\omega) \equiv \partial p_0(\omega)/\partial y_1$.

To simplify the analysis we shall examine in detail the case where $l \gg L$; this enables the base of the cavity to be ignored in calculating the motion of the vortex sheet. To do this we first perform the calculation for a compressible fluid within the cavity, when $Q \neq 0$, and obtain the solution for incompressible flow by considering the limit $\omega l/c_0 \to 0$. When $\omega l/c_0$ is small, motion of the sheet may be assumed to excite acoustic depth modes within the cavity, which vary only with x_2. By imposing the condition that the normal velocity must vanish at the base $x_2 = -l$, and when interior boundary-layer losses, etc. are neglected, the depth mode pressure p_- near the mouth of the cavity may then be shown to be given by (Pierce 1989)

$$p_- = -\mathrm{i}(\rho_0 c_0 Q/A) \cot(\kappa_0 l), \tag{4.5}$$

where $A = bL$ is the cross-sectional area and $\kappa_0 = \omega/c_0$. When the local motion near the vortex sheet is regarded as incompressible (as before), the small influence of radiation damping can be incorporated by taking the mean pressure above the cavity to consist of p_0 (which varies linearly in the mean flow direction) plus a uniform pressure $\omega\kappa_0\rho_0 Q/2\pi$, which vanishes as $c_0 \to \infty$ (the incompressible limit) and corresponds to the first compressible term in the expansion of (4.1) in powers of $\omega|\boldsymbol{x}|/c_0$. Thus, we can write

$$p_+ = x_1 p_0' + \omega\kappa_0\rho_0 Q/2\pi, \tag{4.6}$$

where, without loss of generality, it has been assumed that $p_0 = 0$ at $x_1 = 0$.

In the disturbed state the net pressure above the vortex sheet is given by the first of the general equations (2.2). When ζ does not depend on the spanwise variable y_3, the pressure on the upper surface of the vortex sheet averaged over the span, can be written

$$p = p_+ + \frac{\rho_0 U^2}{\pi s}\left(\sigma + \mathrm{i}\frac{\partial}{\partial\xi}\right)^2 \int_{-1}^{1} \zeta(\eta)\{\ln|\xi-\eta| + \mathscr{L}(\xi,\eta)\}\,\mathrm{d}\eta \quad (|\xi| \equiv |x_1/s| < 1), \tag{4.7}$$

where the notation is the same as in §§2, 3 and $\mathscr{L}(\xi,\eta)$ is defined as in (2.5).

Similarly, since ζ does not depend on x_3, the incompressible motion induced by the vortex sheet in the cavity just below the sheet can be determined by conformal transformation, by expressing it as an integral involving the potential of a line source injecting fluid into a semi-infinite, uniform duct. The net pressure on the lower face of the vortex sheet is then found to be given by

$$p = p_- - \frac{\rho_0 U^2 \sigma^2}{\pi s} \int_{-1}^{1} \zeta(\eta)\{\ln|\xi-\eta| + \mathscr{L}_c(\xi,\eta)\}\,\mathrm{d}\eta \quad (|\xi| < 1), \tag{4.8}$$

where

$$\mathscr{L}_c(\xi,\eta) = \ln\left(\frac{4\sin\{\tfrac{1}{4}\pi(\xi-\eta)\}\cos\{\tfrac{1}{4}\pi(\xi+\eta)\}}{\xi-\eta}\right).$$

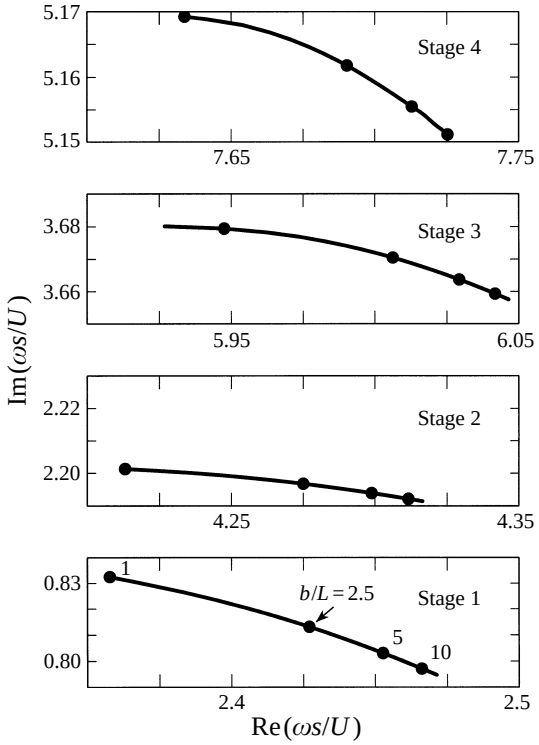

FIGURE 12. Poles of $D(\omega)$ in the upper half-plane for the first four shallow-cavity operating stages ($L = 2s$).

The equation of motion of the sheet is obtained by equating the pressures (4.7) and (4.8), and can be cast in the form

$$\left[\sigma^2+\left(\sigma+\mathrm{i}\frac{\partial}{\partial\xi}\right)^2\right]\int_{-1}^{1}\zeta(\eta)\{\ln|\xi-\eta|+\mathscr{L}(\xi,\eta)\}\,\mathrm{d}\eta$$

$$+\sigma^2\int_{-1}^{1}\zeta(\eta)\{\mathscr{L}_c(\xi,\eta)-\mathscr{L}(\xi,\eta)\}\,\mathrm{d}\eta=-\pi s(p_+-p_-)/\rho_0 U^2\quad(|\xi|<1).\quad(4.9)$$

This equation is integrated with respect to the differential operator in the square brackets to yield

$$\int_{-1}^{1}\zeta(\eta)\{\ln|\xi-\eta|+\mathscr{L}(\xi,\eta)+\mathfrak{C}(\xi,\eta)\}\,\mathrm{d}\eta+\lambda_1\exp(\mathrm{i}\sigma_1\xi)+\lambda_2\exp(\mathrm{i}\sigma_2\xi)=\mathfrak{J}(\xi)\quad(|\xi|<1),$$

(4.10)

where $\mathfrak{J}(\xi)$ is known in terms of $p_\pm$, the coefficients λ_1, λ_2 are constants of integration, σ_1, σ_2 are the Kelvin–Helmholtz wavenumbers, defined as in (2.6), and

$$\mathfrak{C}(\xi,\eta)=\tfrac{1}{2}\sigma\int_{-1}^{1}\{\mathscr{L}_c(\mu,\eta)-\mathscr{L}(\mu,\eta)\}\exp\{\mathrm{i}\sigma(\xi-\mu)-\sigma|\xi-\mu|\}\,\mathrm{d}\mu.$$

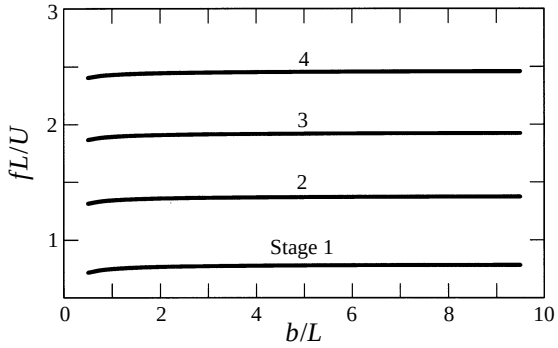

FIGURE 13. Predicted dependence of the shallow cavity Strouhal number fL/U on aspect ratio b/L ($L = 2s$) at infinitesimal mean flow Mach number.

n	Theory: $b/L = 5$ fL/U	Ahuja & Mendoza (1995) fL/U
1	0.78	0.7
2	1.37	1.1
3	1.92	1.7
4	2.45	2.5

TABLE 2

If we now set

$$\zeta = \frac{\mathrm{i}\pi Q Z_A}{2\omega s}\zeta_A - \frac{\pi p_0'}{2\rho_0\omega^2}\zeta_D, \tag{4.11}$$

where $Z_A \equiv \mathrm{i}\kappa_0/2\pi - \cot(\kappa_0 l)/\kappa_0 A$ is the acoustic impedance of the cavity entrance in the absence of flow, then the dimensionless displacement ζ_A is the solution of (4.10) that satisfies the Kutta condition at $\xi = -1$ for $\mathfrak{J}(\xi) \equiv 1$, and ζ_D is the corresponding solution when $\mathfrak{J}(\xi) = \xi - i/\sigma$.

The numerical solutions of these equations can be used to evaluate the moments

$$I_\alpha = \int_{-1}^{1} \zeta_\alpha(\eta)\,\mathrm{d}\eta, \quad M_\alpha = \int_{-1}^{1} \eta\zeta_\alpha(\eta)\,\mathrm{d}\eta \quad (\alpha = D \text{ or } A), \tag{4.12}$$

whose values depend on the shape of the cavity and the hydrodynamic flow, but are independent of fluid compressibility (i.e. c_0). Using (4.4) and the relation $Q = -i\omega b\int_{-s}^{s}\zeta(y_1)\,\mathrm{d}y_1$, we can then evaluate

$$D = \tfrac{1}{2}\pi bs\,\frac{\frac{1}{2}\pi bZ_A[I_A M_D - I_D M_A] - M_D}{1 - \frac{1}{2}\pi bZ_A I_A}, \quad Q = \frac{(\mathrm{i}\pi bsp_0'/2\rho_0\omega) I_D}{1 - \frac{1}{2}\pi bZ_A I_A}. \tag{4.13}$$

These expressions are applicable for compressible motion within the cavity. When $\kappa_0 l \to 0$, the acoustic impedance $Z_A \to \infty$, but all of the other components on the right-hand sides of (4.13) are unchanged. It follows that $Q \to 0$, as expected, and that D tends to a limiting value given by

$$\frac{D}{\frac{1}{2}\pi bs^2} = \frac{[M_A I_D - M_D I_A]}{I_A} \equiv \Gamma'(\omega) - \mathrm{i}\Delta'(\omega), \tag{4.14}$$

where Γ' and $-\Delta'$ are non-dimensional real and imaginary parts of D.

The variations of Γ' and Δ' with real values of $\sigma \equiv \omega s/U$ are illustrated in figure 11(*b*) for a cavity aspect ratio $b/L = 1$. It may be verified that energy from the applied pressure gradient p_0' is absorbed by the mean flow when $\Delta' > 0$, i.e. for σ less than about 2.8. The motion is unstable, however, since $D(\omega)$ has poles in $\mathrm{Im}\,(\omega) > 0$ which occur in distinct bands (analogous to the stages for aperture and edge tones) as b/L varies. These bands are shown in figure 12 for the first four operating stages; the real and imaginary parts of σ increase approximately by $\frac{1}{2}\pi$ in passing from one stage to the next, as for the aperture tones, and figure 13 shows that the Strouhal number $fL/U = \mathrm{Re}\{\sigma/\pi\}$ increases very slowly with aspect ratio for the first four stages, in broad agreement with the observations of Ahuja & Mendoza (1995). Table 2 reveals further an excellent numerical correspondence with Strouhal number estimates (in the third column of the table) obtained by extrapolating to zero Mach number the experimental data for shallow cavity tones presented by Ahuja & Mendoza in their figure 2.2.

5. Conclusion

Fluid–structure interactions involving the incidence of shear layers and jets on edges and corners are frequently sources of narrow-band acoustic radiation. This radiation is conventionally associated with the formation of discrete vortices in the shear layer or jet whose interaction with the structure generates an impulsive pressure that triggers the formation of new vortices and completes a self-sustaining feedback cycle. In this paper we have investigated idealized, linearized models of these interaction for shear flows over wall apertures and cavities, and for the jet–edge interaction. The operating stages of the oscillations have been identified with poles in the upper half of the complex frequency plane of an appropriate impulse response function; for apertures and the jet–edge interaction the response function coincides with the Rayleigh conductivity of the 'window' spanned by the shear flow; for shallow wall cavities (where there is no net volume flux through the mouth of the cavity) the response function is the cavity drag coefficient.

We have argued that, the correct deduction from linear theory is that the real parts of these complex poles correspond to the frequencies of possible self-sustaining cycles of the fluid–structure interaction, generally leading to the production of sound of the same frequency. Detailed predictions have been made of the Strouhal numbers of the first four operating stages of rectangular wall apertures and shallow cavities. Very limited experimental evidence exists to confirm these results, but the wall cavity predictions are in good agreement with extrapolations to zero Mach number of data from measurements in air. On the other hand, jet–edge interactions have been studied extensively, and our Strouhal number predictions are in excellent agreement with data derived from several experimental investigations. Additional support for the validity of linear theory is provided by a comparison of predicted edge-tone Strouhal numbers with those given by a nonlinear theory that depends on a single empirical constant. Linear and nonlinear theories yield identical predictions for a single, fixed value of this constant.

When the fluid–structure interaction takes place in the neighbourhood of a cavity resonator, exemplified by the jet–edge interaction in a flue organ pipe, the instability poles (which are shifted slightly because of the interaction with the resonator) are augmented by a system of poles whose real parts are close to the resonance frequencies of the cavity. The resonator will 'speak' at one or more of these frequencies when the pole lies in the upper frequency plane, a condition that can be satisfied provided the

power supplied via the jet–edge interaction exceeds that lost by radiation from the open ends and by other dissipative mechanisms within the cavity.

This work was sponsored by the Office of Naval Research under Grant N00014-95-1-0318, administered by Dr Patrick L. Purtell. It is a pleasure to acknowledge the benefit of discussions with Dr William K. Blake and Dr Maurice M. Sevik during the preparation of the paper.

REFERENCES

Ahuja, K. K. & Mendoza, J. 1995 Effects of cavity dimensions, boundary layer, and temperature on cavity noise with emphasis on benchmark data to validate computational aeroacoustic codes. *NASA Contractor Report: Final Report Contract* NAS1-19061, Task 13.

Blake, W. K. & Powell, A. 1986 The development of contemporary views of flow-tone generation. In *Recent Advances in Aeroacoustics* (ed. A. Krothapali & C. A. Smith), pp. 247–325. Springer.

Brown, G. B. 1937*a* The vortex motion causing edge tones. *Proc. Phys. Soc. Lond.* **49**, 493–507.

Brown, G. B. 1937*b* The mechanism of edge-tone production. *Proc. Phys. Soc. Lond.* **49**, 508–521.

Bruggeman, J. C. 1987 Flow induced pulsations in pipe systems. PhD thesis, Eindhoven University of Technology.

Bruggeman, J. C., Hirschberg, A., van Dongen, M. E. H., Wijnands, A. P. J. & Gorter, J. 1989 Flow induced pulsations in gas transport systems: analysis of the influence of closed side branches. *J. Fluids Engng* **111**, 484–491.

Burroughs, C. B. & Stinebring, D. R. 1994 Cavity flow tones in water. *J. Acoust. Soc. Am.* **95**, 1256–1263.

Crighton, D. G. 1985 The Kutta condition in unsteady flow. *Ann. Rev. Fluid Mech.* **17**, 411–445.

Crighton, D. G. 1992 The jet edge-tone feedback cycle; linear theory for the operating stages. *J. Fluid Mech.* **234**, 361–392.

Curle, N. 1953 The mechanics of edge-tones. *Proc. R. Soc. Lond.* A**216**, 412–424.

Durbin, P. A. 1984 Resonance in flows with vortex sheets and edges. *J. Fluid Mech.* **145**, 275–285.

East, L. F. 1966 Aerodynamically induced resonance in rectangular cavities. *J. Sound Vib.* **3**, 277–287.

Hardin, J. C. & Pope, D. S. 1995 Sound generation by flow over a two-dimensional cavity. *AIAA J.* **33**, 407–412.

Heller, H. H. & Bliss, D. B. 1975 The physical mechanism of flow-induced pressure fluctuations in cavities and concepts for their suppression. *AIAA Paper* 75-491.

Holger, D. K., Wilson, T. A. & Beavers, G. S. 1977 Fluid mechanics of the edgetone. *J. Acoust. Soc. Am.* **62**, 1116–1128.

Holger, D. K., Wilson, T. A. & Beavers, G. S. 1980 The amplitude of edgetone sound. *J. Acoust. Soc. Am.* **67**, 1507–1511.

Howe, M. S. 1981 The influence of mean shear on unsteady aperture flow, with application to acoustical diffraction and self-sustained cavity oscillations. *J. Fluid Mech.* **109**, 125–146.

Howe, M. S. 1996 Low Strouhal number instabilities of shear flow over wall apertures. *Boston University Rep.* AM-96-008; submitted to *J. Acoust. Soc. Am.*

Howe, M. S., Scott, M. I. & Sipcic, S. R. 1996 The influence of tangential mean flow on the Rayleigh conductivity of an aperture. *Proc. R. Soc. Lond.* A **452**, 2303–2317.

Komerath, N. M., Ahuja, K. K. & Chambers, F. W. 1987 Prediction and measurement of flows over cavities – a survey. *AIAA paper* 87-022.

Kriesels, P. C., Peters, M. C. A. M., Hirschberg, A., Wijnands, A. P. J., Iafrati, A., Riccardi, G., Piva, R. & Bruggeman, J. C. 1995 High amplitude vortex induced pulsations in gas transport systems. *J. Sound Vib.* **184**, 343–368.

Lamb, H. 1932 *Hydrodynamics*, 6th edn, reprinted 1994. Cambridge University Press.

Lepicovsky, J. & Ahuja, K. K. 1983 Some new results on edge tone oscillations in high speed subsonic jets. *AIAA Paper* 83-0665.

LIGHTHILL, M. J. 1958 *An Introduction to Fourier Analysis and Generalised Functions*. Cambridge University Press.

MÖHRING, W. 1975 On flows with vortex sheets and solid plates. *J. Sound Vib.* **38**, 403–412.

PETERS, M. C. A. M. 1993 Aeroacoustic sources in internal flows. PhD thesis, Eindhoven University of Technology.

PIERCE, A. D. 1989 *Acoustics, An Introduction to its Principles and Applications*. American Institute of Physics.

POWELL, A. 1961 On the edgetone. *J. Acoust. Soc. Am.* **33**, 395–409.

RAYLEIGH, LORD 1945 *Theory of Sound*, vol. 2. Dover.

ROCKWELL, D. 1983 Oscillations of impinging shear layers. *AIAA J.* **21**, 645–664.

ROSSITER, J. E. 1962 The effect of cavities on the buffeting of aircraft. *Royal Aircraft Establishment Tech. Mem.* 754.

SCOTT, M. I. 1995 The Rayleigh conductivity of a circular aperture in the presence of a grazing flow. Master's thesis, Boston University.

TAM, C. K. W. & BLOCK, P. J. W. 1978 On the tones and pressure oscillations induced by flow over rectangular cavities. *J. Fluid Mech.* **89**, 373–399.

TITCHMARSH, E. C. 1952 *Theory of Functions*, 2nd corrected edn. Oxford University Press.